SUPPLEMENTARY MATERIALS AND METHODS

Generation and identification of K5.N-Smad7 mice

After birth, transgenic mice were identified by PCR analysis of tail DNA. The K5.N-Smad7 was identified by PCR using forward primer 1 specific for the 5′ K5 vector (5′ TACA GCTCCTGGGCAACGTG 3′) and reverse primer 2 specific for the human N-SMAD7 (5′ TTGAGCACCGAGTGCGTGAG 3′). The PCR product was positive for the N-SMAD7 transgene at ~350 base pair.

Animal models

For transgenic mice, K5.Smad7 mice were bred into C57BL/6 background as previously reported (He et al., 2001). K5.N-Smad7 mice were maintained in the FVB/NJ background. Male and female transgenic mice aged 8–10 weeks and their wild-type littermates were used for the imiquimod (IMQ) test. Considering the sex bias of IMQ response for the FVB/NJ strain (Swindell et al., 2017), both females and males were included in the tests. No gender differences were observed in the IMQ tests in K5.N-Smad7 mice.

Mice used for Tat–PYC–SMAD7 treatment were purchased from the Jackson Laboratory (Bar Harbor, ME). Female C57BL/6J-Tyr<c-2J>/J (albino C57BL/6J) (JAX000058), female BALB/CJ (JAX000651), female and male FVB/NJ (JAX001800) mice aged 8–10 weeks were used to establish the IMQ model. Mice received a daily topical dose of 62.5 mg IMQ cream (5%) (Aldara; 3M Pharmaceuticals, Saint Paul, MN) on the shaved back for 4 consecutive days (van der Fits et al., 2009). Female C57BL/6J-Tyr<c-2J>/J (JAX000058) mice aged 8 weeks were used for atopic dermatitis and tape-stripping models. DNFB-induced atopic dermatitis was induced by topical painting using 100 μl 0.15% DNFB (D1529, Sigma-Aldrich, St. Louis, MO) in acetone/olive oil (3:1) daily to the shaved back skin from day 1 to day 3. Tape stripping was induced by applying 20 strokes of transparent tape (Scotch, 3M Pharmaceuticals) across the shaved and depilated (Nair, Church & Dwight, Ewing Township, NJ) dorsal skin (Di Domizio et al., 2020; Gregorio et al., 2010).

Animal models. An objective PASI scoring system developed previously was used to score the severity of IMQ skin by observers blinded from study groups (van der Fits et al., 2009). Skin thickness of DNFB-induced atopic dermatitis lesion was measured in duplicate using a micrometer (Mitutoyo, Kawasaki, Japan). For phenotypic evaluation, at least three independent experiments were conducted with 4–5 mice in each group of the experiment.

Tat–PYC–SMAD7 treatment

Tat–PYC–SMAD7 was generated and formulated as previously described (Boss et al., 2022). Tat–PYC–SMAD7 is a recombinant protein that contains the PY and C domains of SMAD7 (203–426 amino acid) fused with a cell-permeable Tat tag (Li et al., 2019; Luo et al., 2019). A hemagglutinin epitope was added to the C-terminus of Tat–PYC–SMAD7 to enable tracking of the protein. Hydroxypropyl cellulose gel (1% Klucel HF, Ashland Global, Wilmington, DE) containing 1X PBS and 30% glycerol was used as the base gel. Vehicle and Tat–PYC–SMAD7 gel were formulated by carefully mixing the protein buffer or the protein stock, respectively, with the base gel at a 1:2 ratio. All mice were randomly grouped to assure minimal environmental variation during the experiment. Twenty-four hours after experimental day 1, when the skin barrier was compromised, skin lesions (~2 cm^2) were treated with 30 μl vehicle gel or Tat–PYC–SMAD7 gel (0, 0.125, 0.25, 0.5 μg daily dose) using a pipette equipped with filter tips. Mice were held manually until all the gel was absorbed completely. The treatment was administered to the mice from day 2 to day 6. On day 6, mice were killed 2 hours after the final dose of the treatment. Treated skin tissues from identical locations of each mouse were collected for further histological evaluation or for lysis or RNA extraction. Because tape strokes cause uneven skin lesions in the tape-stripping model, mice with similar lesion severity were paired before the treatment and underwent subsequent pairwise evaluation.

In vivo small interfering RNA transfection

In vivo transfection of IL-22RA2 small interfering RNA (siRNA) or control siRNA into the skin was performed by subcutaneous injection of 100 ng ON-TARGETplus Mouse IL22RA2 siRNA (L-057637-01, Dharmacon, Lafayette, CO) or nontargeting siRNA Pool (D-001810-10, Dharmacon) using in vivo-jetPEI delivery reagent (201-10G, Polyplus, Illkirch-Graffenstaden, France) 1 day before the IMQ application. The siRNA–in vivo-jetPEI complex was freshly prepared, following the manufactory's instruction, and the injection volume was 50 μl per mouse.

Cell culture and transfection

HaCaT cells were maintained in a DMEM culture medium supplemented with 10% fetal bovine serum and 1% Primocin (InvivoGen, San Diego, CA). The coding region of human PYC–SMAD7 (203–426 amino acid) with a 5′ hemagglutinin-tag–coding sequence was inserted into pCMV6-Entry as a NotI/XhoI fragment and verified by Sanger sequencing. This construct was transfected into HaCaT keratinocytes using Lipofectamine 3000 transfection reagent (Invitrogen, Waltham, MA) followed by selection with 1 mg/ml G418 to generate stably expressing cells. Surviving colonies were subcloned using trypsin-soaked cloning discs and placed into 24-well plates and expanded. Expression of PYC–SMAD7 in individual subclones was verified by immunostaining, western blot, and qPCR as described below. HaCaT keratinocytes or PYC–SMAD7–transfected HaCaT cells (i.e., PYC–HaCaT) at 70% confluency were changed into Keratinocyte-SFM medium (catalog number 10724-011, Gibco, Billings, MT). A total of 100 nM of ON-TARGETplus Human CEBPB (1051) siRNA-SMARTpool (L-006423-00, Dharmacon) or nontargeting siRNA Pool (D-001810-10, Dharmacon) was transfected using 5 μl DharmaFECT 1 Transfection Reagent (Dharmacon) for 12-well plates. Cells were lysed 48 hours after siRNA transfection and subjected to western blotting analyses to determine knockdown efficiency.

RNA-sequencing and microarray data analysis

Tissue samples for RNA-sequencing analysis were harvested and immediately frozen in liquid nitrogen and stored at −80 °C until the time of analysis. RNA was harvested using an RNA Plus mini Kit (74136, Qiagen, Hilden, Germany). Sequencing and library preparation was performed by the Genomics and Microarray Shared Resource at the University

of Colorado Denver Cancer Center (Aurora, CO). PolyA selection was used for library preparation, and sequencing was performed on an Illumina NovaSEQ 6000 with 2 × 200 paired-end reads at a depth of 80 million reads per sample. Quality control was conducted by FastQC (https://www.bioinformatics.babraham.ac.uk/projects/fastqc/) and FastQ Screen (https://www.bioinformatics.babraham.ac.uk/projects/fastq_screen/). RNA-sequencing reads were adapter trimmed and clipped using BBDuk (BBMap – Bushnell B. – sourceforge.net/projects/bbmap/). Trimmed sequences were aligned to mouse genome GRCm38.p6 (release 96) with STAR (Dobin et al., 2013). Raw counts of identified genes were quantified and referenced against gene-stable identifications for the following analysis. Differential expression was calculated by fitting the negative binomial generalized log-linear model and conducting the likelihood ratio test (McCarthy et al., 2012) on the trimmed mean of M values (Robinson and Oshlack, 2010) normalized count data using the R package edgeR (Robinson et al., 2010). The false discovery rate was calculated for multiplicity correction using the Benjamini–Hochberg method (Benjamini and Hochberg, 1995).

Gene set enrichment analyses were performed using preranked gene set enrichment analyses (Subramanian et al., 2005) and Enrichr (Chen et al., 2013) implemented by the GSEApy package (version 0.10.3, https://doi.org/10.5281/zenodo.3748085). The preranked gene set enrichment analyses utilized all identified genes preranked by the negative logarithm of the *P*-value with the sign of $\log_2$ fold change. The Enrichr handled a list of differentially expressed genes with *P*-values <0.01 and absolute $\log_2$ fold changes >0.6. The analyzed pathways were from Gene Ontology biological process, Kyoto Encyclopedia of Genes and Genomes, and hallmark gene set databases.

Microarray data of human skin inflammation treatments were collected from the National Center for Biotechnology Information Gene Expression Omnibus database including atopic dermatitis (GSE133477) (Bissonnette et al., 2019) and psoriasis (GSE85034) (Correa da Rosa et al., 2017; Goldminz et al., 2015). Because IL-22RA2 has a direct impact on IL-22/Jak/signal transducer and activator of transcription 3 signaling (Huber et al., 2012), datasets from clinical trials using Jak inhibitors were avoided. Both trials have RNA samples from patients collected before and after the treatment analyzed by microarray analysis. *IL22RA2* gene expression levels were compared at the same lesional location for individual patients before and after the treatment. A two-sided paired samples *t*-test was used to evaluate potential changes in the gene expression intensity before and after treatments.

qPCR and western blotting

RNA Plus mini Kit (number 74136, Qiagen) was used to extract total RNA from cells or tissue samples. Relative family genes were determined with TaqMan assays (Thermo Fisher Scientific, Waltham, MA) using Brilliant II QRT-PCR 1-step Master Mix kit (600809, Agilent Technologies, Santa Clara, CA) for each reaction. Ct values of the gene of interest and *GAPDH* were used to determine relative fold change by $2^{-\Delta\Delta Ct}$. Proteins were harvested with RIPA buffer (9806S, Cell Signaling Technology, Danvers, MA) supplemented with a protease inhibitor cocktail (4693124001, Roche, Basel, Switzerland). Western blotting was performed using standard protocols and detected using a ChemiDoc Imaging System (Bio-Rad Laboratories, Hercules, CA). Antibodies and TaqMan assays are described in Supplementary Table S1.

Immunohistochemistry, simmunofluorescence, immunocytochemistry, and histological analysis

Immunofluorescence and immunohistochemistry staining was performed on formalin-fixed paraffin-embedded skin sections, and immunocytochemistry was conducted for detection of protein expression and localization in cultured cells. Immunofluorescence/immunohistochemistry staining was performed as previously described (Han et al., 2013). Samples were counterstained with DAPI and Alexa Fluor–conjugated secondary antibodies (Thermo Fisher Scientific) or SignalStain Boost IHC Detection Reagent (8114 and 63707, Cell Signaling Technology) with DAB Quanto Detection System (TA-125-QHDX, Epredia, Kalamazoo, MI) for detection. For immunocytochemistry, cells seeded in chamber slides reaching 50% confluency were stained using an Immunofluorescence Application Solutions Kit (12727, Cell Signaling Technology), following the manufacturer's instructions. The primary antibodies used are detailed in Supplementary Table S1. The number of mice with or without microabscess was quantified through the entire H&E section per mouse. Each group contained five mice, and a skin section was taken from each mouse for evaluation. Sequential ×10 or ×20 images along the basement membrane were quantified and averaged per sample using Olympus cellSens Dimension software. Nuclear Ki-67– and phosphorylated signal transducer and activator of transcription 3–positive cells were quantified as the percentage of positive cell area per total epidermal area. CD31-, S100A8-, CD3-, Ly6G-, and F4/80-positive cells were quantified as the percentage of positive cell area per total skin area.

Multiplex Spectral Imaging

Multiplex Spectral Imaging analysis was performed on the Vectra platform (Caliper Life Sciences, Waltham, MA) at the Human Immune Monitoring Shared Resource within the University of Colorado Human Immunology and Immunotherapy Initiative core. Formalin-fixed paraffin-embedded tissues were deparaffinized, heat treated in antigen retrieval buffer, blocked, and consecutively incubated with primary antibodies for cytokeratin 5 (1:100), CD3 (1:50), Ly6G (1:500), and F480 (1:100), followed by horseradish peroxidase–conjugated secondary antibody polymer and horseradish peroxidase–reactive OPAL fluorescent reagents (Opals 480, 570, 620, and 780, respectively) on a Leica Bond RX autostainer (Leica Biosystems, Wetzlar, Germany). Slides were heat treated in antigen retrieval buffer and blocked between each staining step and were counterstained with spectral DAPI. Whole-slide scans were collected on the Vectra 3.0 automated instrument using the ×10 objective. Multispectral images were collected using the ×20 objective with a 0.5-μ resolution. inForm software, version X (Akoya Biosciences, Marlborough, MA), was used to unmix adjacent fluorochromes, subtract autofluorescence, and evaluate staining morphology and cell marker expression. The primary antibodies used are detailed in Supplementary Table S1.

ELISA

Samples of tissue lysis, cell supernatants, and plasma were subjected to ELISA. Tissue specimens were homogenized in PBS with a protease inhibitor cocktail (4693124001, Roche) and underwent one freeze-thaw cycle in 1% Triton X to obtain tissue lysis. Tissue lysate concentrations were determined by BCA assay and adjusted to be equal before detection. Levels of IL-22, IL-22RA2, IL-24, IL-33, and CXCL1 were detected using ELISA kits according to the manufacturer's instructions. A total of 100 μl samples were used for detection. The ELISA kits used are listed in Supplementary Table S1.

Chromatin immunoprecipitation assays

Transcriptional factor C/EBPβ that regulates IL-22RA2 expression was predicted through chromatin immunoprecipitation-sequencing information obtained from https://academic.oup.com/database/article/doi/10.1093/database/bax028/3737828. Chromatin immunoprecipitation assays were performed using the SimpleChIP Plus Enzymatic Chromatin IP Kit (Magnetic Beads) (9005, Cell Signaling Technology). We isolated the DNA–protein complex from HaCaT or PYC–HaCaT clones. For chromatin immunoprecipitation, we incubated 5 μg sheared chromatin with protein-G magnetic beads and 2 μg each of rabbit antibodies to hemagglutinin-Tag (3724, Cell Signaling Technology), C/EBPβ (NBP1-46179, Novus Biologicals, Centennial, CO), and a negative control rabbit IgG (2729, Cell Signaling Technology). We used eluted DNA from the protein–DNA complex for PCR analyses and compared C/EBPβ/HA binding with the IL-22RA2 promoter by chromatin immunoprecipitation band intensities on gel images or by quantitative PCR using SimpleChIP Universal qPCR Master Mix (88989, Cell Signaling Technology). Primers used to amplify the 580 kb IL-22RA2 promoter region designed by Integrated DNA Technologies (Coralville, IA) were 5′-CTT GGTACCTAGCCGACAATTAG-3′ (sense) and 5′-TCACTCC TGATCTCCTGACC-3′ (antisense).

Statistical analysis

The statistical comparison between two experimental groups was performed using unpaired two-tailed *t*-tests or Mann–Whitney test. Multiple comparisons were performed either using two-way ANOVA with Sidak's or Tukey's multiple comparisons test or one-way ANOVA with Tukey's multiple comparisons tests. Contingency data were compared using the chi-square test. Data were presented as the mean ± SEM. Data are representative of at least 2–3 independent experiments, with 3–6 samples per group in each.

SUPPLEMENTARY REFERENCES

Benjamini Y, Hochberg Y. Controlling the false discovery rate: a practical and powerful approach to multiple testing. J Royal Stat Soc Ser B 1995;57:289–300.

Bissonnette R, Pavel AB, Diaz A, Werth JL, Zang C, Vranic I, et al. Crisaborole and atopic dermatitis skin biomarkers: an intrapatient randomized trial. J Allergy Clin Immunol 2019;144:1274–89.

Boss MK, Ke Y, Bian L, Harrison LG, Lee BI, Prebble A, et al. Therapeutic intervention using a Smad7-based Tat protein to treat radiation-induced oral mucositis. Int J Radiat Oncol Biol Phys 2022;112:759–70.

Chen EY, Tan CM, Kou Y, Duan Q, Wang Z, Meirelles GV, et al. Enrichr: interactive and collaborative HTML5 gene list enrichment analysis tool. BMC Bioinformatics 2013;14:128.

Correa da Rosa J, Kim J, Tian S, Tomalin LE, Krueger JG, Suárez-Fariñas M. Shrinking the psoriasis assessment gap: early gene-expression profiling accurately predicts response to long-term treatment. J Invest Dermatol 2017;137:305–12.

Di Domizio J, Belkhodja C, Chenuet P, Fries A, Murray T, Mondéjar PM, et al. The commensal skin microbiota triggers type I IFN-dependent innate repair responses in injured skin. Nat Immunol 2020;21:1034–45.

Dobin A, Davis CA, Schlesinger F, Drenkow J, Zaleski C, Jha S, et al. STAR: ultrafast universal RNA-seq aligner. Bioinformatics 2013;29:15–21.

Goldminz AM, Suárez-Fariñas M, Wang AC, Dumont N, Krueger JG, Gottlieb AB. CCL20 and IL22 messenger RNA expression after adalimumab vs methotrexate treatment of psoriasis: A randomized clinical trial. JAMA Dermatol 2015;151:837–46.

Gregorio J, Meller S, Conrad C, Di Nardo A, Homey B, Lauerma A, et al. Plasmacytoid dendritic cells sense skin injury and promote wound healing through type I interferons. J Exp Med 2010;207:2921–30.

Han G, Bian L, Li F, Cotrim A, Wang D, Lu J, et al. Preventive and therapeutic effects of Smad7 on radiation-induced oral mucositis. Nat Med 2013;19:421–8.

He W, Cao T, Smith DA, Myers TE, Wang XJ. Smads mediate signaling of the TGFbeta superfamily in normal keratinocytes but are lost during skin chemical carcinogenesis. Oncogene 2001;20:471–83.

Huber S, Gagliani N, Zenewicz LA, Huber FJ, Bosurgi L, Hu B, et al. IL-22BP is regulated by the inflammasome and modulates tumorigenesis in the intestine. Nature 2012;491:259–63.

Kanehisa M, Furumichi M, Tanabe M, Sato Y, Morishima K. KEGG: new perspectives on genomes, pathways, diseases and drugs. Nucleic Acids Res 2017;45:D353–61.

Li F, Bian L, Iriyama S, Jian Z, Fan B, Luo J, et al. Smad7 ameliorates TGF-beta-mediated skin inflammation and associated wound healing defects but not susceptibility to experimental skin carcinogenesis. J Invest Dermatol 2019;139:940–50.

Luo J, Bian L, Blevins MA, Wang D, Liang C, Du D, et al. Smad7 promotes healing of radiotherapy-induced oral mucositis without compromising oral cancer therapy in a xenograft mouse model. Clin Cancer Res 2019;25:808–18.

McCarthy DJ, Chen Y, Smyth GK. Differential expression analysis of multifactor RNA-Seq experiments with respect to biological variation. Nucleic Acids Res 2012;40:4288–97.

Robinson MD, McCarthy DJ, Smyth GK. edgeR: a Bioconductor package for differential expression analysis of digital gene expression data. Bioinformatics 2010;26:139–40.

Robinson MD, Oshlack A. A scaling normalization method for differential expression analysis of RNA-seq data. Genome Biol 2010;11:R25.

Subramanian A, Tamayo P, Mootha VK, Mukherjee S, Ebert BL, Gillette MA, et al. Gene set enrichment analysis: a knowledge-based approach for interpreting genome-wide expression profiles. Proc Natl Acad Sci U S A 2005;102:15545–50.

Swindell WR, Michaels KA, Sutter AJ, Diaconu D, Fritz Y, Xing X, et al. Imiquimod has strain-dependent effects in mice and does not uniquely model human psoriasis. Genome Med 2017;9:24.

van der Fits L, Mourits S, Voerman JS, Kant M, Boon L, Laman JD, et al. Imiquimod-induced psoriasis-like skin inflammation in mice is mediated via the IL-23/IL-17 axis. J Immunol 2009;182:5836–45.

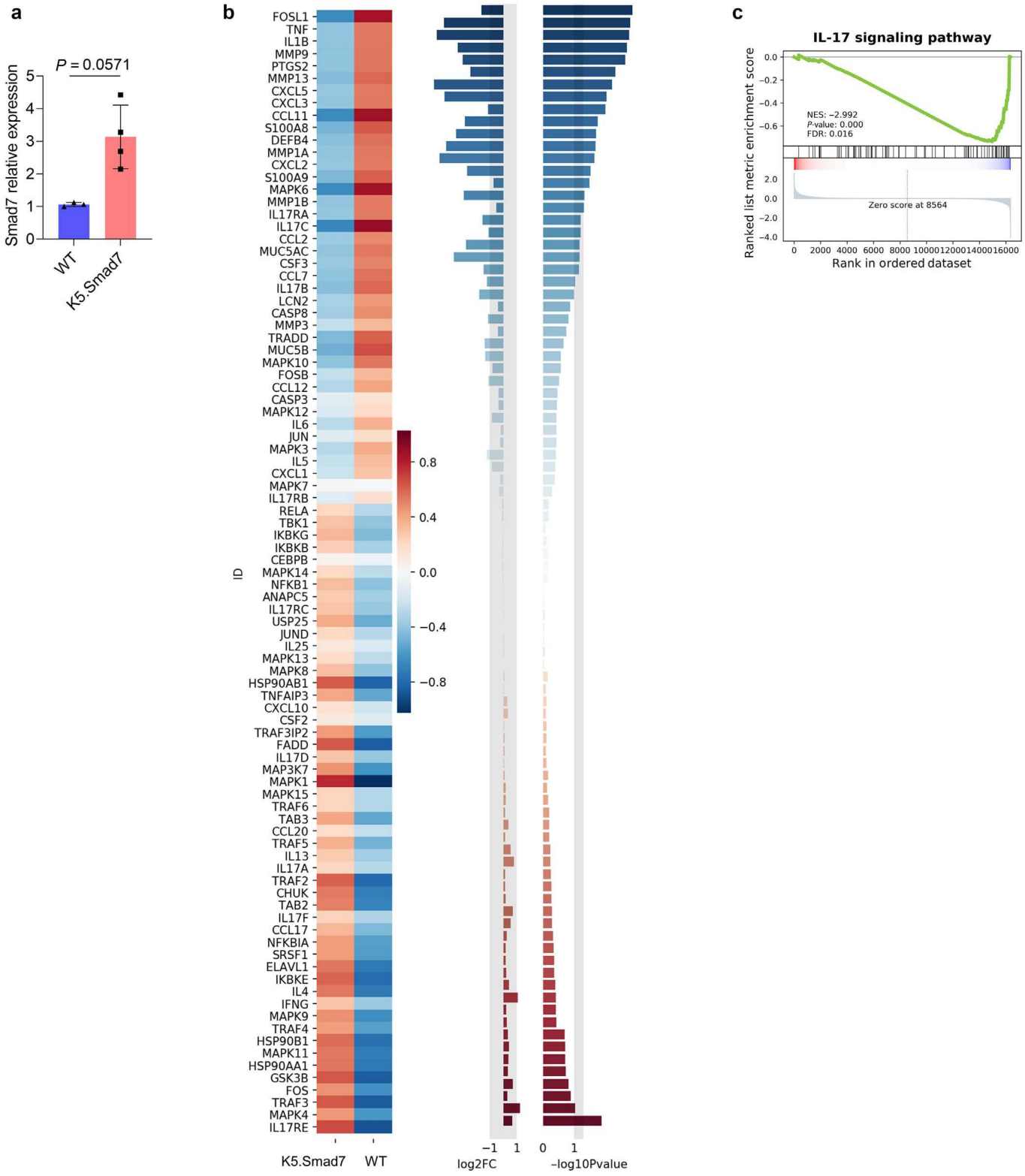

Supplementary Figure S1. Expression of SMAD7 and analysis of IL-17 signaling pathway in K5.Smad7 IMQ skin samples. (**a**) SMAD7-relative expression in IMQ skin of WT of K5. Smad7 mice on experimental day 6. Skin samples from WT (n = 3) and K5.Smad7 (n = 4) mice were qualified using two-tailed Mann–Whitney *U* test for statistics. Data are representative of at least three independent experiments, with 3–6 samples per group in each. Data represent the mean ± SEM. Presented is a heatmap with a bar plot of the *P*-value and FC of (**b**) signature genes and (**c**) enrichment plot for IL-17 signaling pathway by comparing mean transcriptome levels of K5.Smad7 IMQ skin sample (n = 4) with those of WT IMQ skin samples (n = 3) on day 6. K5.Smad7 denotes keratin 5 *Smad7*-transgenic mice. FC, fold change; FDR, false discovery rate; IMQ, imiquimod; NES, normalized enrichment score; WT, wild type.

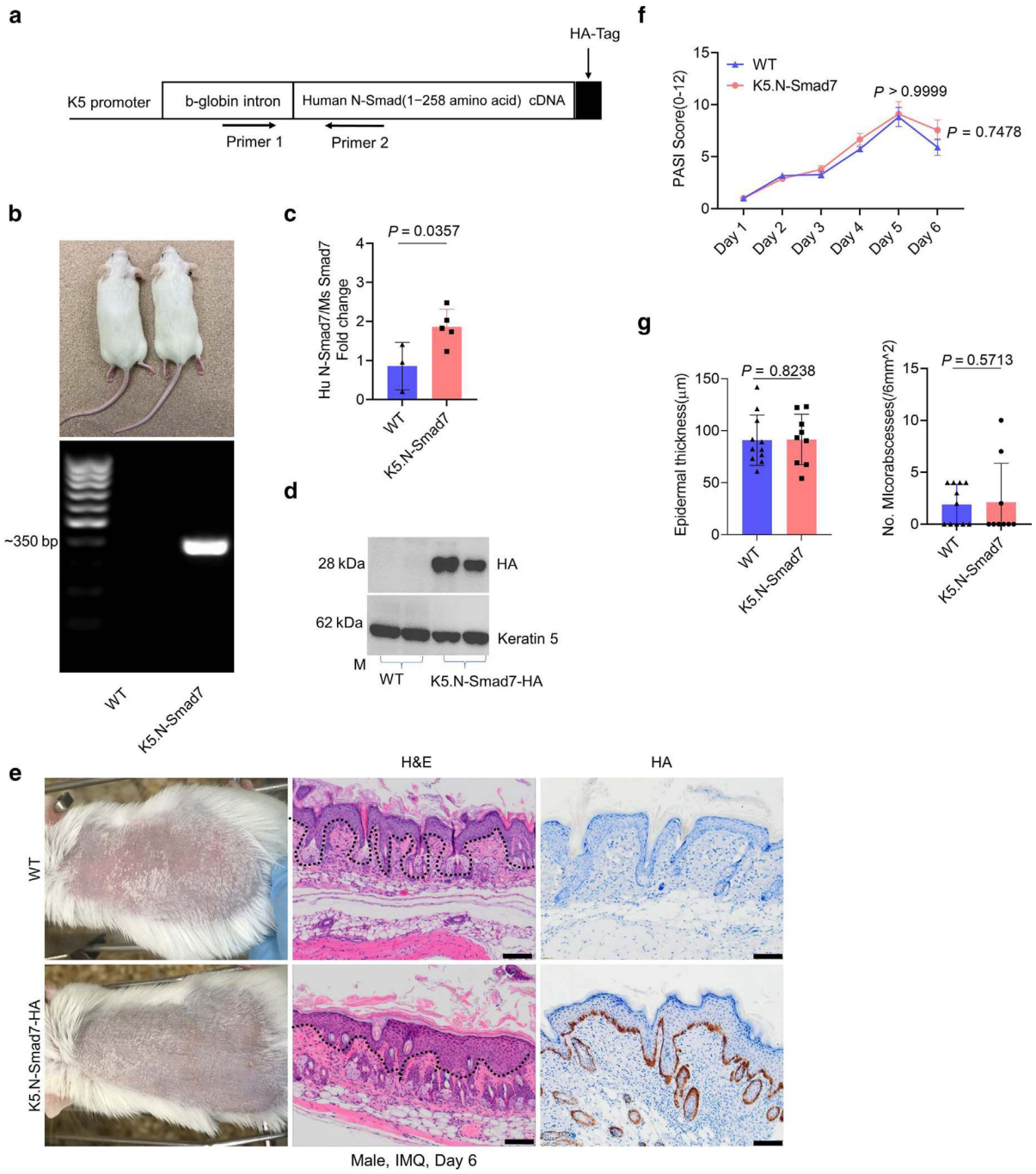

Supplementary Figure S2. K5.N-Smad7 skin developed a skin phenotype similar to that of WT skin by IMQ challenge. (**a**) K5.N-Smad7 transgene. (**b**) Representative gross images and corresponding genotyping of WT littermate and K5.N-Smad7. (**c**) qPCR and (**d**) western blot indicating the transgenic expression levels of N-SMAD7 in IMQ skin of K5.N-Smad7 compared with that in WT IMQ skin. (**e**) Representative gross images (left), corresponding H&E skin sections (middle), and IHC staining for HA (right) of IMQ-induced lesions on experimental day 6 from WT and K5.N-Smad7 mice. The N-*Smad7* transgene contains an HA tag, so IHC against HA was performed in **e**. (**f**) PASI scores of IMQ-induced skin phenotypes of the WT and K5.N-Smad7 mice on days 1–6 during IMQ application. (**g**) Average epidermal thickness and number of microabscesses in H&E. Dotted lines: epidermal–dermal boundary. Bars = 100 μm for all slides. Five skin samples from each group were qualified using (**f**) two-way ANOVA test or (**g**) two-tailed unpaired *t*-test for statistics. Data are representative of at least three independent experiments, with 3–4 samples per group in each. Data represent the mean ± SEM. K5.N-Smad7 denotes keratin 5 N-*Smad7*-transgenic mice. HA, hemagglutinin; IHC, immunohistochemistry; IMQ, imiquimod; WT, wild type.

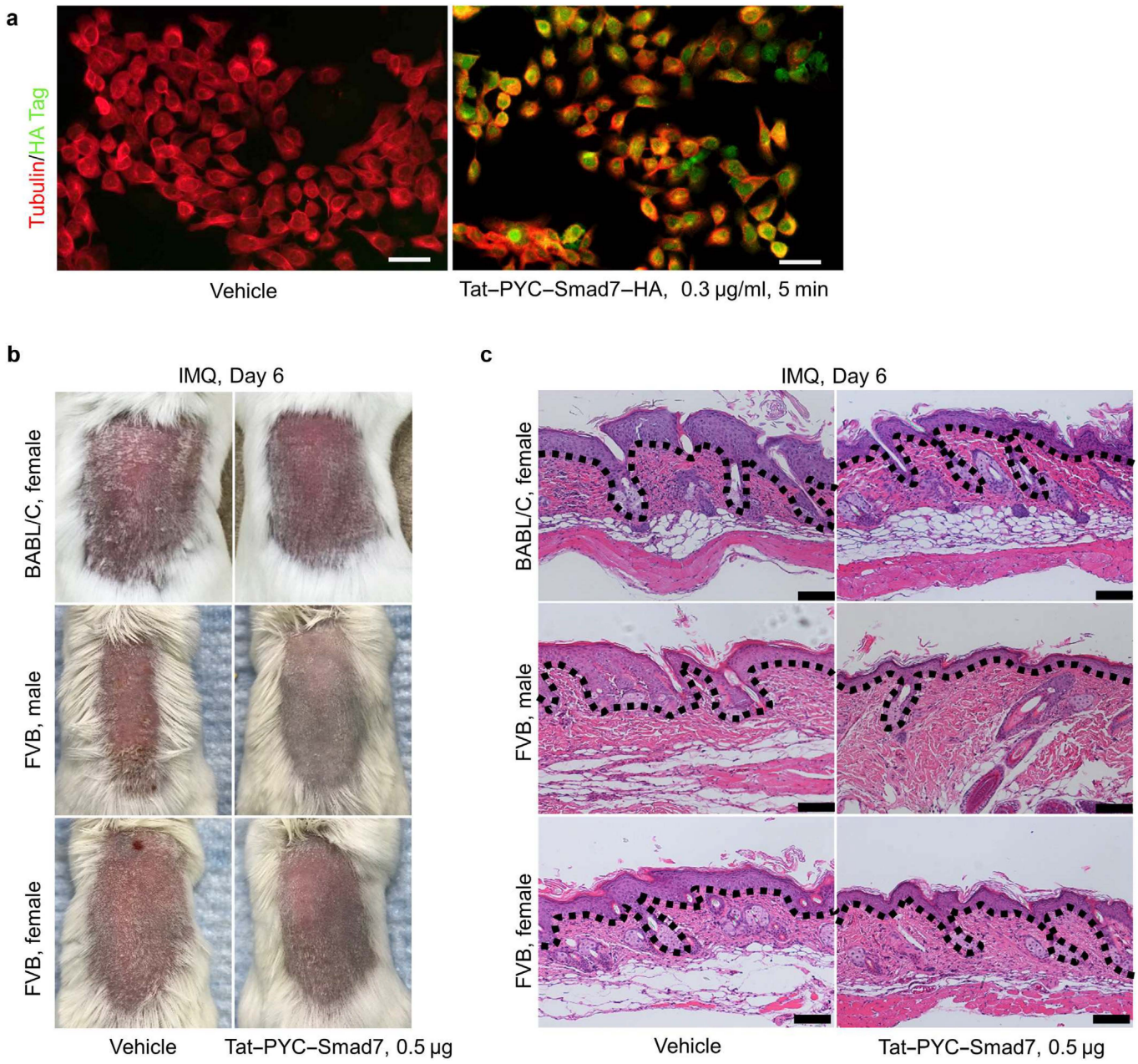

Supplementary Figure S3. Anti-inflammatory effects of Tat–PYC–SMAD7 on both Th1/17- and Th2-type inflammation in IMQ mouse models. (**a**) IF staining using HA antibody (green) showing Tat–PYC–SMAD7 entering the nucleus of HaCaT keratinocytes (red); the left image is vehicle control. (**b**) Representative gross images and (**c**) corresponding H&E images of IMQ-induced lesions on experimental day 6 from female BALB/cJ and female and male FVB/NJ mice with daily treatment of vehicle control or Tat–PYC–SMAD7 at the dose of 0.5 μg starting from experimental day 2. Dotted lines: epidermal–dermal boundary. Bars = 100 μm for all the slides. HA, hemagglutinin; IF, immunofluorescence; IMQ, imiquimod; min, minute; Th, T helper.

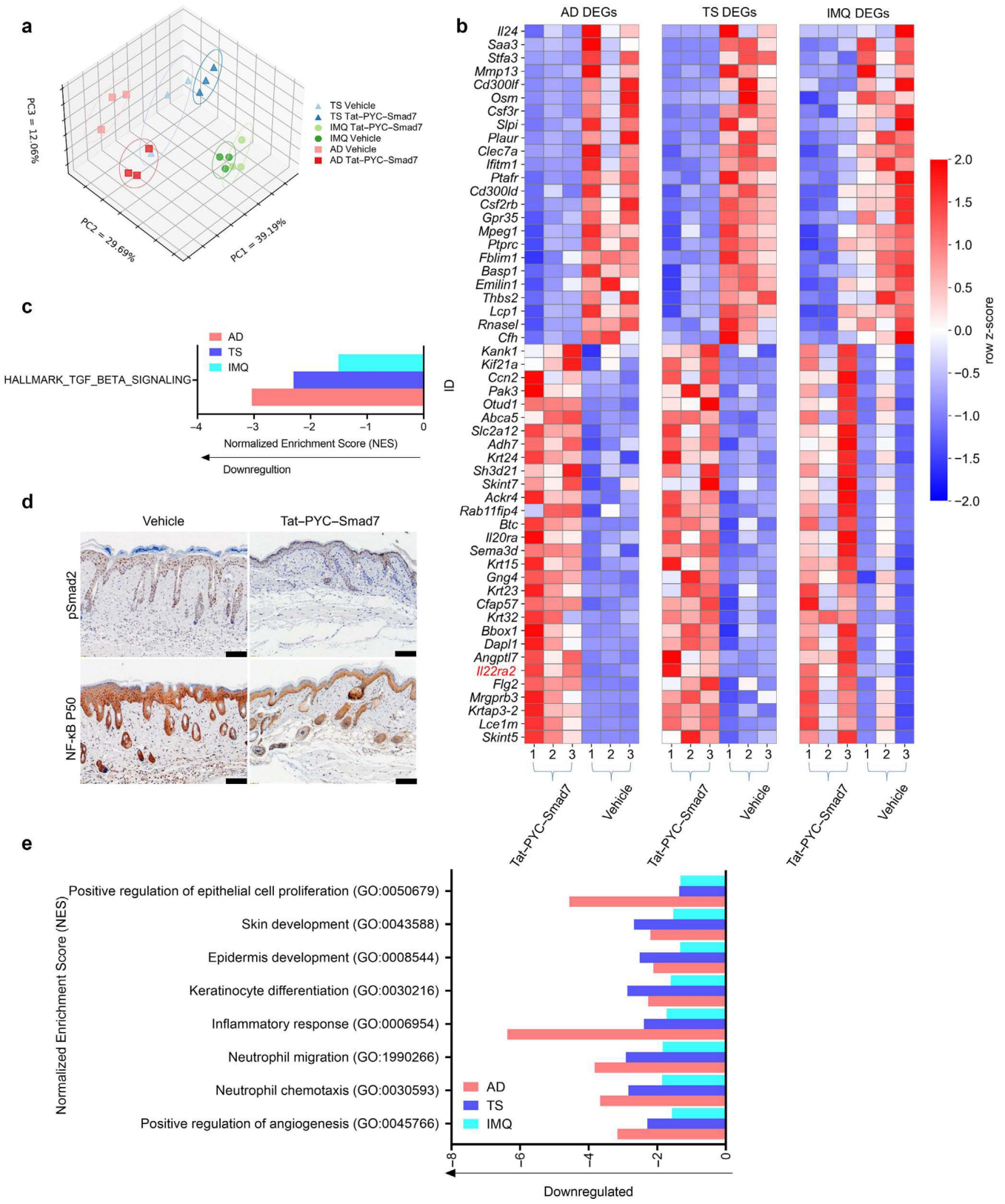

Supplementary Figure S4. RNA-seq analysis for samples of IMQ, AD, and TS skin with Tat–PYC–SMAD7 treatment. (**a**) Principal components analysis of RNA-seq data of IMQ skin, IMQ, AD, and TS skin from albino B6 with the treatment of vehicle control (n = 3) or Tat–PYC–SMAD7 at the dose of 0.5 μg (n = 3) on experimental day 6. (**b**) Representative shared DEGs ($P < 0.01$; $-0.6 > \text{LogFC} > 0.6$) of IMQ, AD, and TS skin challenged by Tat–PYC–SMAD7 treatment. (**c**) Graphs show the most highly enriched Hallmark categories in the transcriptome changes of IMQ, AD, and TS skin with Tat–PYC–SMAD7 treatment. (**d**) Representative images of IHC staining on the skin sections of IMQ skin lesions. (**e**) Graphs show the most highly enriched GO categories in the transcriptome changes of IMQ, AD, and TS skin with Tat–PYC–SMAD7 treatment normalized to those of vehicle treatment. Bars= 100 μm for all slides. AD, atopic dermatitis; DEG, differentially expressed gene; FC, fold change; GSEA, gene set enrichment analysis; GO, Gene Ontology; IHC, immunohistochemistry; IMQ, imiquimod; PC, principal component; pSmad2, phosphorylated SMAD2; RNA-seq, RNA sequencing; TS, tape stripping.

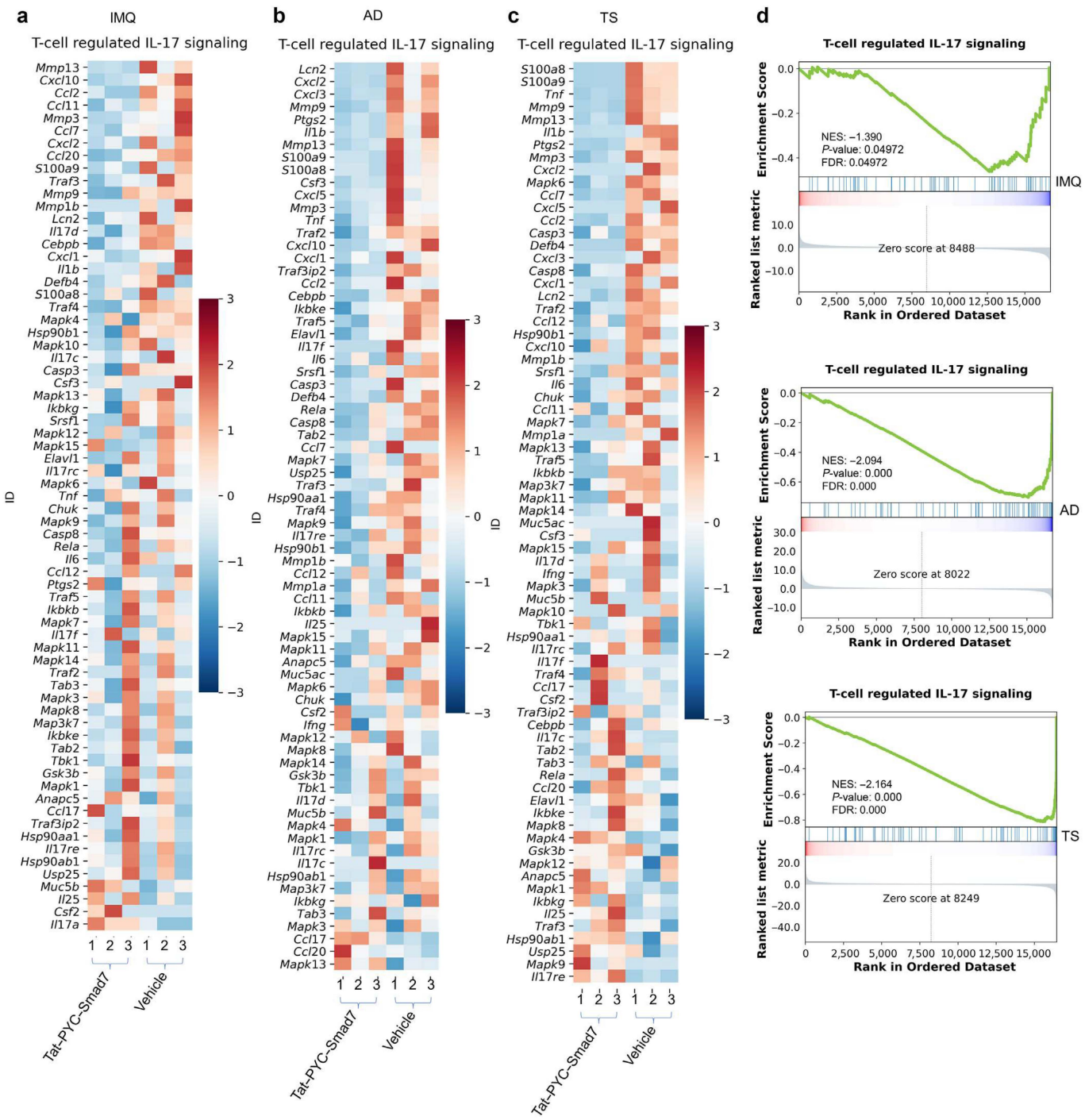

Supplementary Figure S5. GSEA in KEGG term comparing the transcriptomes of IMQ, AD, and TS skin with Tat−PYC−SMAD7 with those for vehicle treatment. (**a**–**c**) Heatmap of signature genes and (**d**) enrichment plot for T-cell−regulated IL-17 signaling pathway by GSEA in KEGG term (Kanehisa et al., 2017) comparing transcriptomes of IMQ, AD, and TS skin with Tat−PYC−SMAD7 with those for vehicle treatment on day 6. AD, atopic dermatitis; FDR, false discovery rate; GSEA, gene set enrichment analysis; IMQ, imiquimod; KEGG, Kyoto Encyclopedia of Genes and Genomes; NES, normalized enrichment score; TS, tape stripping.

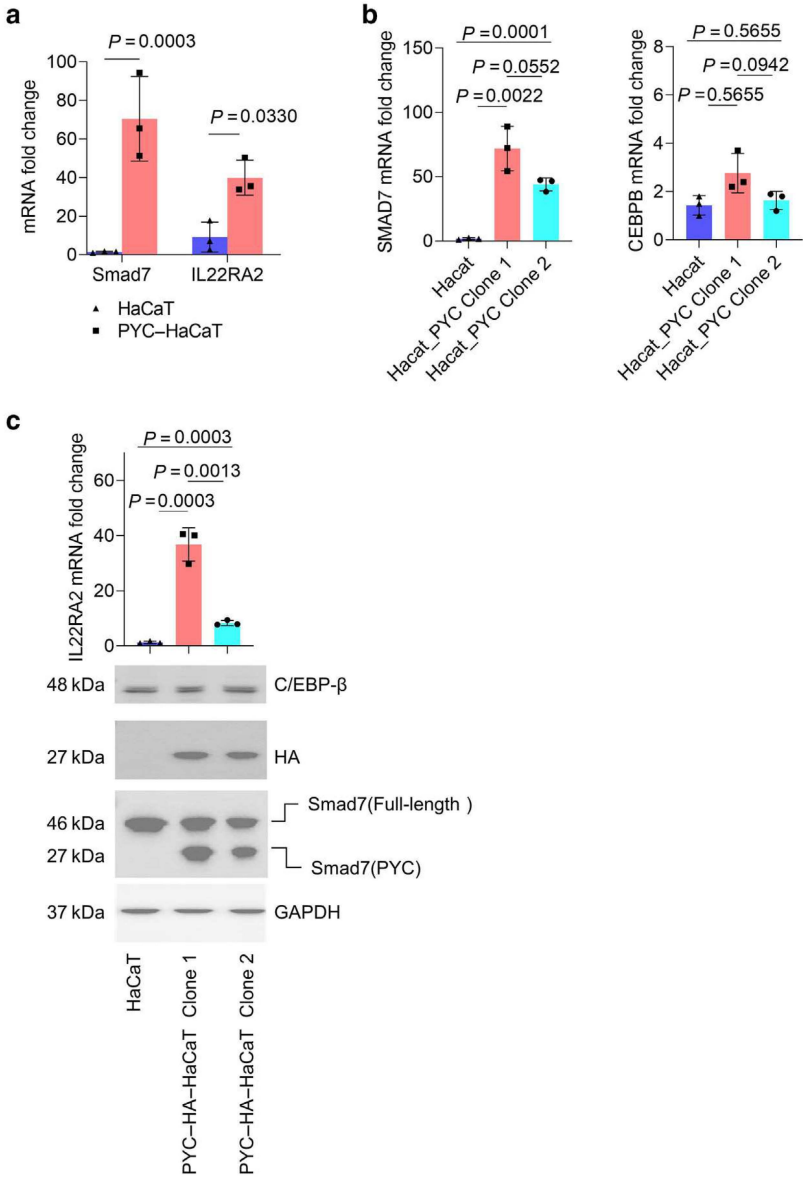

Supplementary Figure S6. mRNA and protein expression levels of SMAD7 and IL-22RA2 in HaCaT and PYC–HaCaT cells. (**a**) mRNA fold change by qPCR using probes recognizing C-terminal SMAD7 and IL-22RA2 (n = 3 for each group). (**b, c**) mRNA fold change by qPCR and protein levels by western blot using cell lysis from HaCaT and PYC–HaCaT clone 1 and 2 cells. Data are representative of three independent experiments. Data represent the mean ± SEM. PYC–HaCaT denotes HA–PYC–SMAD7–transfected HaCaT cells. HA, hemagglutinin; IHC, immunohistochemistry.

Supplementary Table S1. Reagents Used in the Experiments that Are Not Listed in the Methods Section

Reagents	Manufacturer	Catalog Number	Application
Taqman Assay Mouse SMAD7	Thermo Fisher Scientific	Mm00492189_cn	qPCR
TaqMan Assay Mouse SMAD7	Thermo Fisher Scientific	Mm00484741_m1	qPCR
Taqman Assay Human SMAD7	Thermo Fisher Scientific	Hs00998191_m1	qPCR
Taqman Assay Human SMAD7	Thermo Fisher Scientific	Hs00998193_m1	qPCR
TaqMan Assay Mouse IL22RA2	Thermo Fisher Scientific	Mm01192969_m1	qPCR
TaqMan Assay Human IL22RA2	Thermo Fisher Scientific	Hs00364814_m1	qPCR
TaqMan Assay Human CEBPB	Thermo Fisher Scientific	Hs00270923_s1	qPCR
TaqMan Assay Mouse GAPDH	Thermo Fisher Scientific	Mm99999915_g1	qPCR
TaqMan Assay Human GAPDH	Thermo Fisher Scientific	Hs02758991	qPCR
Mouse IL-22RA2 ELISA Kit	Cloud-Clone Corp	SEE767Mu	ELISA
Human IL-22BP DuoSet ELISA	R&D Systems	DY1087-05	ELISA
Mouse IL-24 DuoSet ELISA	R&D Systems	DY2786-05	ELISA
Mouse IL-33 DuoSet ELISA	R&D Systems	DY3626-05	ELISA
Mouse CXCL1DuoSet ELISA	R&D Systems	DY453-05	ELISA
Mouse IL-22 Elisa Kit	BioLegend	50-169-531	ELISA
IL-22RA2 Antibody	Invitrogen	PA1-21359	ICC, IHC
SMAD7 Antibody	Novus Biological	NBP1-87728	IHC, WB
C/EBPβ	Novus Biological	NBP1-46179	ICC, WB
NF-kB p105/p50 (p Ser337) Antibody	Novus Biological	NB100-82074	IHC
Keratin 14 Antibody	BioLegend	50-112-9910	IF
Ki-67 (D3B5) Antibody	Cell Signaling Technology	12202	IHC
CD31 (PECAM-1) Antibody	Cell Signaling Technology	77699	IHC
S100A8 (E4F8V) Antibody	Cell Signaling Technology	47310	IHC
Phosphorylated STAT3 (Tyr705) Antibody	Cell Signaling Technology	9145	IHC, WB
HA-Tag (C29F4) Antibody	Cell Signaling Technology	3724	ICC, IF, WB
pSMAD2 (Ser465, Ser467) Antibody	Invitrogen	44-244G	IHC
CD3 (D4V8L) Antibody	Cell Signaling Technology	99940	MSI
F4/80 (D2S9R) Antibody	Cell Signaling Technology	70076	MSI
Ly-6G (E6Z1T) Antibody	Cell Signaling Technology	87048	MSI
Cytokeratin 5 Antibody	Abcam	ab64081	MSI

Abbreviations: HA, hemagglutinin; ICC, immunocytochemistry; IF, immunofluorescence; IHC, immunohistochemistry; MSI, multiplex spectral imaging; pSMAD2, phosphorylated SMAD2; STAT3, signal transducer and activator of transcription 3; WB, western blot.